Accepted for publication in Building and Environment
DOI: 10.1016/j.buildenv.2015.05.008

Stable reduced-order models for pollutant dispersion in the built environment

Lieven Vervecken[a,b], Johan Camps[a], Johan Meyers[b]

[a] *SCK•CEN, Belgian Nuclear Research Centre, Boeretang 200, BE-2400 Mol, Belgium*
[b] *Department of Mechanical Engineering, KU Leuven, Celestijnenlaan 300, BE-3000 Leuven, Belgium*

Abstract

In order to limit the impact of accidental releases of hazardous pollutants into the atmosphere, there is a need for an accurate near-range atmospheric dispersion modeling approach that is suitable for on-line risk management. Computational Fluid Dynamics (CFD) has proven to be a promising tool for atmospheric dispersion studies at the near-range. However, the relatively long computing times currently prohibit the use of CFD for real-time purposes. Therefore, we present in this work an effective model reduction method that is based on the projection of the original model, which solves the transient advection-diffusion equation on a steady background velocity field, onto a Krylov subspace by means of the Arnoldi algorithm. This allows to construct a reduced order model (ROM) from an accurate CFD model that is guaranteed to be stable. The algorithm is formulated in such a way that the ROM can be derived using any CFD software package, commercial or non-commercial. The accuracy of the ROM is illustrated by performing a series of simulations of a time-dependent pollutant release at the Doel nuclear power station, located to the north of Antwerp (Belgium). A comparison between the results obtained using the ROM after initialization, and the original CFD model shows a reduction of a factor of 2500 in computational time, leading to a ROM that runs 25 times faster than real-time without a significant loss in accuracy. In terms of computational cost, the ROM is a factor 10^5 less expensive than the original CFD model.

Keywords: Computational Fluid Dynamics (CFD), Dispersion, Arnoldi algorithm, Reduced Order Model (ROM)

1. Introduction

The impact of accidental atmospheric releases of hazardous pollutants on the health of the people exposed remains of serious concern [1]. Predicting the time-dependent dispersion of such releases in the atmosphere through the use of numerical models can help to develop plans of response to emergencies. Furthermore, when the runtime is sufficiently short, these models can be used in on-line risk management tools (see, e.g., Ref. [2], or Ref. [3]). While Gaussian-based and Lagrangian models are well established for the latter, Leelőssy et al. [4] identified that there is currently no accurate near-range atmospheric dispersion modeling approach available which complies with this short runtime.

Computational Fluid Dynamics (CFD) has proven to be a promising technique for atmospheric dispersion studies at the near-range [5, 6, 7, 8]. This is in particularly true for the built environment where the complex geometry

Email addresses: lieven.vervecken@sckcen.be (Lieven Vervecken), johan.meyers@mech.kuleuven.be (Johan Meyers)

can result in complex dispersion patterns [9, 10, 11, 12]. Unfortunately, CFD-based models require relatively long computing times which currently prohibit their use for real-time purposes [13, 14]. In this context, Senocak et al. [15] focused on reducing the simulation time by improving the numerical methods and parallel computing strategies. Gowardhan et al. [16] chose to trade some of the accuracy for a gain in simulation speed by simplifying the model. In the current work, we take a different approach by developing a reduced order model (ROM) from a CFD model, thereby greatly reducing the computational time. We consider the particular case of a neutral buoyant gas, that is injected with a time-dependent source rate and dispersed given known steady wind conditions and site geometry. In such a system, the background velocity field can be precomputed using CFD, and used as an input to a three-dimensional time-dependent convection-diffusion equation with a transient source term.

The goal of model order reduction (MOR) is to reduce the degrees of freedom (DOF) of a large size model to a very small size while maintaining the key behavior of the model [17]. Extensive discussions on MOR methods are presented by Baur et al. [17], Lucia et al. [18] and Antoulas et al. [19]. In the following, we focus on MOR methods dedicated for sparse, linear time-invariant systems such as we encounter in our work (cf. §2.1). The DOF for CFD applications is typically in the order of 10^6 and higher. This is far beyond the practical limit for Truncated Balanced Realization and Hankel Norm Approximation methods, two frequently used ROM methods for linear, time-invariant systems [20]. Instead, Krylov-subspace projection-based ROM methods have shown to be a viable option for such systems [17, 20, 21]. Many algorithms exist for construction of the Krylov subspaces (see, e.g., Ref. 22 or Ref. 23) but two frequently encountered algorithms are the Arnoldi method and the Lanczos method. Nour-Omid et al. [24] compared both methods for the solution of convection-diffusion problems in a Finite Element Method framework. They concluded that the Arnoldi is the method of choice for convection dominated problems. Other examples of the application of the Arnoldi method are presented by Woodbury et al. [25] with the simulation of the contaminant transport in an aquifer, Zhang and Woodbury [26] with a study on the contaminant transport in porous media, Willcox et al. [27] with the development of a ROM for turbomachinery and Wang et al. [28] who developed a ROM for the three-dimensional thermal analysis of microfluidic systems. The degrees of freedom in these applications were all limited to $10^3 - 10^5$, which is considerably lower than required for three-dimensional pollution-dispersion studies as considered in the current work. Nevertheless, all these studies demonstrated significant reductions in required computational cost when solving the corresponding ROM.

Therefore, we apply the Arnoldi method to the simulation of pollutant transport in a built environment. We show that the resulting ROM is guaranteed stable and suitable for faster than real-time atmospheric dispersion assessments. In addition, the algorithm for the construction of the ROM is formulated independently from the choice of CFD solver, such that it is applicable to both open-source and commercial CFD software packages. The effectiveness of the reduced-order model is demonstrated based on a simulation of a time-dependent pollutant release at the Doel Nuclear Power Station, comparing the ROM results to the high-resolution CFD.

This paper is further organized as follows. First, in section 2, we present the model order reduction methodology and the pollutant dispersion model. Next, in section 3 we detail the simulation cases considered in the current work

and the numerical setup of our simulations. Simulation results are discussed in section 4. Finally, conclusions are presented in section 5.

2. Methodology

In the current section we briefly introduce the continuous and discrete formulation of the pollutant dispersion model in §2.1. Next, the construction of the ROM is presented in §2.2.

2.1. Pollutant dispersion model

Consider the three-dimensional dispersion of a non-buoyant, non-reactive gas in a steady, thermally neutral boundary layer, for a constant wind direction, and known site geometry. In this situation, the three-dimensional velocity field $\langle \boldsymbol{u} \rangle(\boldsymbol{x})$ can be obtained from a standard CFD model, e.g., either based on Reynolds-averaged Navier–Stokes simulations or large-eddy simulations (for practical details, cf. §3.2). The dispersion is then further modeled using a time-dependent three-dimensional advection-diffusion problem. Neglecting the small effect of molecular diffusion, the evolution of the pollutant concentration is described by

$$\frac{\partial c}{\partial t} + \nabla \cdot (\langle \boldsymbol{u} \rangle \, c) = -\nabla \cdot \langle \boldsymbol{u}' c' \rangle + S \tag{1}$$

where c is the concentration, and S the pollutant source term. We model the turbulent diffusion $\langle \boldsymbol{u}' c' \rangle$ with an eddy-diffusivity approach, i.e.

$$-\langle \boldsymbol{u}' c' \rangle \approx \frac{\nu_t}{Sc_t} \nabla c \tag{2}$$

with Sc_t the turbulent Schmidt number, and ν_t the eddy viscosity. The latter is also straightforwardly obtained from a precomputed flow simulation. In the current study we employ $Sc_t = 0.9$ (see, e.g., Ref. [29] for a discussion on values for the turbulent Schmidt number).

Spatial discretization of Eq. (1), e.g., using a finite-volume approach, results in a large coupled system of ordinary differential equations. This system can be written as

$$\frac{\mathrm{d}\tilde{c}}{\mathrm{d}t} = A\tilde{c} + bs \tag{3}$$

where $\tilde{c}(t) \in \mathbb{R}^n$ is the solution vector containing the concentration of every cell in the domain, $b \in \mathbb{R}^n$ is the source vector containing the contribution of every cell to the pollutant source and $s(t)$ is the source magnitude input. In addition, the sparse matrix $A \in \mathbb{R}^{n \times n}$ is the discrete representation of the advection and the diffusion operator, including the spatial boundary conditions. When set up properly, this matrix is negative-definite. Note that in practice, this matrix is not explicitly available, but indirectly coded in the CFD software used to solve Eq. (1).

Algorithm 1 One-sided Arnoldi algorithm to construct a basis of $\mathcal{K}_r(A^{-1}, A^{-1}b)$.

1. Initialize:
   (a) Solve for $\tilde{v}_1^{\dagger}$: $A\tilde{v}_1 = b$
   (b) Set: $v_1 = \frac{\tilde{v}_1}{\|\tilde{v}_1\|}$
2. For $i = 2 \dots r$ do:
   (a) Solve for $\tilde{v}_i^{\dagger}$: A $\tilde{v}_i = v_{i-1}$
   (b) Orthogonalize $\tilde{v}_i$: for $j = 1 \dots i-1$
   $h = \tilde{v}_i v_j$
   $\tilde{v}_i = \tilde{v}_i - h v_j$
   (c) Normalize: $v_i = \frac{\tilde{v}_i}{\|\tilde{v}_i\|}$
3. Set $V = [v_1 v_2 \dots v_r]$
4. Construct $A_r = V^T A V$

† This step can be performed using the CFD package by imposing b or v_{i-1} as source vector in Eq. (3) and solving for the steady state solution.

2.2. Reduced-order model

The purpose of model order reduction (MOR) is to obtain a model of significantly reduced order ($r \ll n$) which, in a certain way, behaves similar to the original full size model [18]. In this view, let $V \in \mathbb{R}^{n\times r}$ be a matrix whose columns form an orthonormal basis of a r-dimensional subspace. Projection of the solution vector c onto this basis can be identified by the approximation $\tilde{c} \approx V c_r$ where c_r is the reduced-order solution vector. Substitution of this approximation in the system of Eq. (3) followed by a Petrov–Galerkin projection using any full-rank matrix $W \in \mathbb{R}^{n\times r}$ results in the reduced order system (see, e.g., Ref. [17] or Ref. [22])

$$W^T V \frac{\mathrm{d}c_r}{\mathrm{d}t} = W^T A V c_r + W^T b s \tag{4}$$

where $A_r = W^T A V \in \mathbb{R}^{r\times r}$ is in general a full matrix, i.e. the sparsity of A is usually lost through the projection. This equation can be fully solved in the reduced-order space with dimension r. Once $c_r(t)$ is obtained, the fine-scale solution can be reconstructed using $\tilde{c} \approx V c_r$.

In this work, we construct the projection matrix V as a basis of the r-th order Krylov subspace in order to provide the moment matching property [30]. The Krylov subspace of order r is defined by

$$\mathcal{K}_r(\tilde{A}, \tilde{b}) = span\{\tilde{b}, \tilde{A}\tilde{b}, \tilde{A}^2\tilde{b}, \dots, \tilde{A}^{r-1}\tilde{b}\} \tag{5}$$

where $\tilde{A}$ is a constant matrix and $\tilde{b}$ is referred to as the starting vector. In order to match the lower part of the frequency domain, we set $\tilde{A} = A^{-1}$ and $\tilde{b} = A^{-1}b$ [31]. In this way, the slow dynamics of the system, i.e. in the order of the main convection time scales, are matched well.

The one-sided Arnoldi method is employed to construct V the basis. By opting for a one-sided method, which implies that $W = V$ and $W^T V = I$ in Eq. (4), the first r moments of the original and the reduced system transfer

Algorithm 2 One-sided Arnoldi algorithm to construct a basis of $\mathcal{K}_r(A^{-1}, A^{-1}b)$.

1. Initialize:
   (a) Solve for $\tilde{v}_1^{\dagger}$: $A\tilde{v}_1 = b$
   (b) Set: $v_1 = \frac{\tilde{v}_1}{\|\tilde{v}_1\|}$ and $x_1 = \frac{b}{\|\tilde{v}_1\|}$
2. For $i = 2 \dots r$ do:
   (a) Solve for $\tilde{v}_i^{\dagger}$: $A\tilde{v}_i = v_{i-1}$
   (b) Set: $\tilde{x}_i = v_{i-1}$
   (c) Orhogonalize $\tilde{v}_i$, and adapt $\tilde{x}_i$: for $j = 1 \dots i-1$
   $h = \tilde{v}_i v_j$
   $\tilde{v}_i = \tilde{v}_i - h v_j$
   $\tilde{x}_i = \tilde{x}_i - h x_j$
   (d) Normalize: $v_i = \frac{\tilde{v}_i}{\|\tilde{v}_i\|}$ and $x_i = \frac{\tilde{x}_i}{\|\tilde{v}_i\|}$
3. Set: $V = [v_1\ v_2\ \dots\ v_r]$ and $X = [x_1\ x_2\ \dots\ x_r]$
4. Construct: $A_R (= V^T A V) = V^T X$

† This step is performed using the CFD package by imposing b or v_{i-1} as source vector in Eq. (3) and solving for the steady state solution.

functions match [30]. The modified Gram-Schmidt implementation of this method is elaborated in Algorithm 1 for a single-input system [32]. The algorithm generates a vector v_i which results from the recursive orthogonalization of the vector $A^{-1}v_{i-1}$ with respect to the previously generated orthonormal vectors. In order to avoid computing the inverse of the matrix A, the linear system $A\tilde{v}_i = v_{i-1}$ is solved to obtain $\tilde{v}_i$. In this way, only r linear systems need to be solved instead of n systems required to compute the inverse. This algorithm can be readily extended towards multiple input systems (see, e.g., Ref. [22] or Ref. [31]).

The A-matrix in Eq. (3) is often not, or only partly, accessible within the CFD package. This can be due to restricted access to the source code, or due to the solution methodology employed by the software package. The latter is for instance the case in OpenFOAM where non-orthogonality in the mesh is accounted for by adding additional source terms to the right-hand side of Eq. (3) instead of increasing the bandwidth of the solution matrix. Thus, if A is not explicitly available, it becomes impossible to directly perform step 4 in Algorithm 1. In order to deal with this, we reformulate the one-sided Arnoldi algorithm in terms of an unknown matrix (A). This results in the introduction of $X \in \mathbb{R}^{n \times r}$ which accounts for the unknown contribution of A to the reduced matrix A_r before the Galerkin projection. The revised algorithm is elaborated in Algorithm 2. The basis V produced by this algorithm and the corresponding reduced matrix A_r are identical to those produced by the classical Arnoldi algorithm. The proof of this equivalence is given in Appendix A. Note that solving $A\tilde{v}_i = v_{i-1}$ for $\tilde{v}_i$ does not require the knowledge of A. This can be achieved by using the CFD package as a black box while imposing v_{i-1} as source vector in Eq. (3) and solving for the steady state solution.

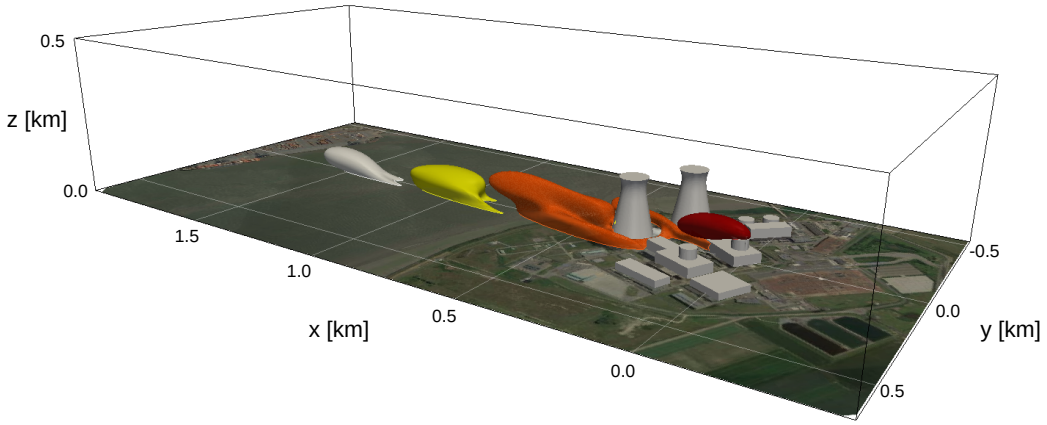

Figure 1: Computational domain. In color, isosurface for the instantaneous concentration $C^+ = 2.5\times10^{-3}$ ($= cUL^2/R$) for case τ_1 at time $t^+ = 5$ (red); $t^+ = 15$ (orange); $t^+ = 25$ (yellow); $t^+ = 35$ (white).

Alternatively, a two-sided method, where $W \neq V$, can be used which matches $2r$ moments (see, e.g., Ref. [33] or Ref. [34]). Clearly, a ROM constructed from a two-sided method has the potential of resulting in a better approximation with respect to a one-sided method because of the higher number of matching moments. However, by taking $W = V$ the definiteness of the original A matrix is preserved. Hence, the projection of a stable system will result in a stable reduced-order model [35, 27]. This is not guaranteed with a two-sided method, and therefore might require the use of stabilization methods (see, e.g., Ref. [36] or Ref. [37]). This is not further explored in the current paper.

3. Case set-up

First, we detail the site considered in the current work in section §3.1. Next, the computational setup used to solve the dispersion problem for both the CFD model and to set up the ROM are elaborated in §3.2.

3.1. Case description

A time-dependent pollutant release at the Doel nuclear power station is the subject of the present study. The geometry of the case studied is shown in figure 1. Pollutant iso-contours of a simulation result at four different time instances are also shown in the figure (cf. below for further details). The nuclear power station includes four cylindrical reactor buildings, two hyperbolic cooling towers with a height of 176 m, and a number of cuboid auxiliary buildings. A uniform surface roughness length $z_0 = 0.01$m, corresponding to short grassland, is set for free ground surface. Two different wind directions are considered in this study, i.e. wind coming from the southwest, which is the prevailing wind direction for this location, and wind coming from the west. For both situations, the friction velocity is set to 0.25 ms^{-1}. This corresponds to a wind speed of 20 km h^{-1} at 74 m altitude. This altitude corresponds to the height of the chimney of Doel 3, the location of the source in the present study.

Table 1: Overview of the length scale, wind speed, dimensional time constant and dimensionless time constant of the three cases simulated.

	L [m]	U [m/s]	τ_i [s]	τ^+ [-]
case τ_1	74	5.568	13.290	1.000
case τ_2	176	6.110	28.806	2.168
case τ_3	500	6.762	73.939	5.564

The coordinate system is chosen such that the coordinate of the source corresponds to $(0, 0, 74\text{m})$ and that the x-axis is in the streamwise direction. The release of the pollutant is simulated as a Gaussian function in time

$$R(t) = a \exp\left(\frac{(t - t_s)^2}{2\tau_i^2}\right) \tag{6}$$

where we set the time of peak emission rate $t_s = 5\tau_i$ and $a = (\tau_i \sqrt{2\pi})^{-1}$ to attain $R(0) \simeq 0$ and $\int_0^\infty R(t')dt' = 1$. In this work, we choose the time constant $\tau_i = L/U$ based on a length scale and the wind speed at this height according to the logarithmic velocity profile. Three length scales are considered, i.e. the chimney height, the cooling tower height and the domain height. The corresponding wind speed and time scales are summarized in table 1. These different scales allow us to evaluate the performance of the ROM for a range of relevant emission scales.

In order to assess the quality of the ROM with respect to the CFD model, two performance measures are used, i.e., the fractional bias (FB) and the normalized mean square error (NMSE) [38, 39]:

$$\text{FB} = 2\frac{\sum\left(C^+_{ROM} - C^+_{CFD}\right)}{\sum\left(C^+_{ROM} + C^+_{CFD}\right)}, \tag{7}$$

$$\text{NMSE} = n\frac{\sum\left(C^+_{ROM} - C^+_{CFD}\right)^2}{\sum C^+_{ROM} \sum C^+_{CFD}}. \tag{8}$$

It is readily seen that a perfect ROM would yield in FB and NMSE = 0. All cells in the whole domain are taken into account for the evaluation of these measures following a paired in space-and-time approach.

Finally, the concentration reported in the current study is normalized as $C^+ = cUL^2/R$ where R is the total amount of pollutant released, L is the height of the chimney and U is the mean wind speed at height L according to the logarithmic velocity profile. Furthermore, distance and time are normalized as $x^+ = xL^{-1}$ and $t^+ = (t - t_s)UL^{-1}$, respectively.

3.2. Computational set up

The transport equations (1) are spatially discretized using second-order schemes on a hexahedral mesh consisting of 8.0 M cells and 10.0 M cells for wind coming from the southwest and the west, respectively. Simulation of the full-size convection-diffusion model is performed using the OpenFOAM finite-volume open-source simulation platform.

In a first step the steady velocity field, and the eddy viscosity are solved. To that end, the Reynolds-averaged Navier–Stokes (RANS) equations are solved with OpenFOAM. Closure is provided by the standard $k-\epsilon$ model [40] in which the model coefficients are chosen in accordance with Richards and Hoxey [41], and also the boundary conditions for the velocity field simulation are set in accordance with Richards and Hoxey [41]. The boundary conditions for the convection-diffusion equation are set to zero at the inlet and Neumann boundary conditions are applied at the other boundaries.

For the implementation of the Arnoldi algorithm and the simulation of the ROM, we use the Petsc library [42, 43, 44]. The order of the ROM is set to 100, but for evaluation of accuracy, we also evaluate reduced-order models with degrees of freedom ranging from 10 up to 150. For the CFD model as well as for the ROM, a second-order Crank-Nicholson scheme is applied for time discretization with a time step $\Delta t^+ = 10^{-3}$. The simulations of the full-size model were carried out on 40 processors distributed over two nodes, installed with Intel Xeon E5-2680 v2 processors and interconnected through DDR infiniband. The simulations of the ROM were carried out on the same machine using only one processor core.

4. Results and discussion

The results of the cases studied are presented in this section by comparing the results of the full CFD model with the ROM. First, in section §4.1, the results of the simulation of case τ_1 with wind coming from the southwest are presented in detail. In addition, it is illustrated that similar results are obtained with wind coming from the west, and for cases τ_2 and τ_3. Subsequently, in §4.2, the obtained reduction in time and computational cost is discussed.

4.1. Simulation results

The dispersion case τ_1 with wind coming from the southwest is used to discuss the general simulation results. We focus the discussion on the concentration at ground level (1 m height) since this is usually of interest in health impact studies (see, e.g., Ref. [38], Ref. [45] and Ref. [46]). The contours of the dimensionless concentration at ground level are shown in Fig. 2 at $t^+ = 5$, 10, 15 and 20 for both the CFD model and the ROM. It is observed that the solution of both models is nearly identical. At $t^+ = 5$, all pollutants are emitted and the plume is advected towards the cooling tower where it splits into two parts. A small part of the plume passes in between the two cooling towers but the major part of the plume passes the cooling tower from the outer side. The maximum concentration at ground level increases to $C^+ = 0.0243$ at $t^+ = 10$ which is found by both models. Afterwards, the concentration steadily decreases with time as a result of turbulent mixing. This illustrates that, notwithstanding the splitting of the plume, the ROM is well capable of reconstructing both the shape and the magnitude of the pollutant concentration.

Fig. 3 shows the evolution of the dimensionless concentration at $t^+ = 10$ for cases τ_1, τ_2 and τ_3 from the point of release along the stream-wise direction (Fig. 3a, Fig. 3c) and along span-wise direction at $x^+ = 7.5$ (Fig. 3b, Fig. 3d) for wind coming from the southwest and the west, respectively. In these graphs, the lines represent the CFD model

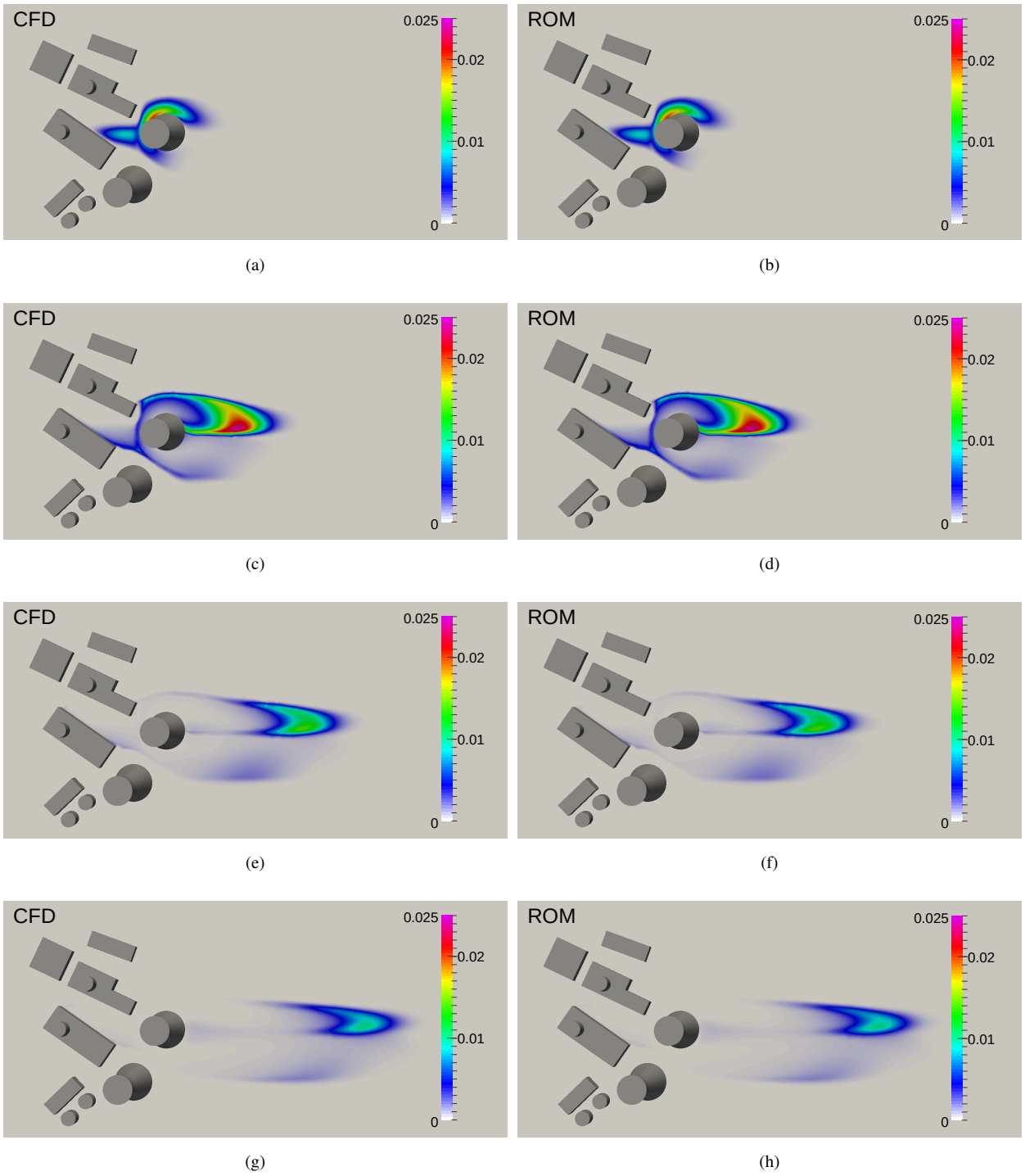

Figure 2: Contours of the dimensionless concentration C^+ ($= cUL^2/R$) observed at ground level (1 m) for case τ_1; (a, b) $t^+ = 5$ ($= (t - t_s)U/L$), (c, d) $t^+ = 10$, (e, f) $t^+ = 15$, (g, h) $t^+ = 20$.

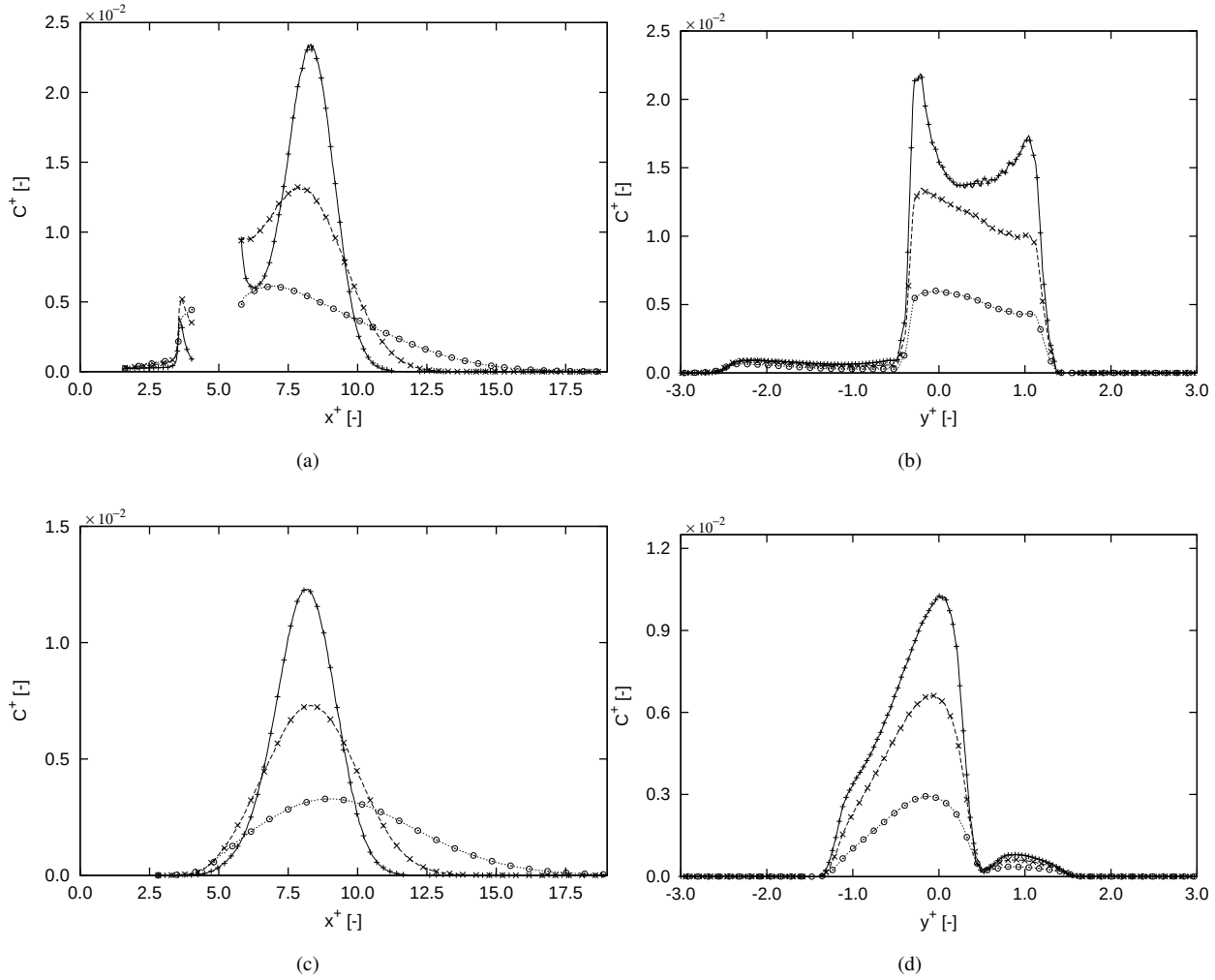

Figure 3: Profiles of the observed dimensionless concentration C^+ ($= cUL^2/R$) observed at ground level (1 m) at $t^+ = 10$ ($= (t - t_s)U/L$). For wind coming from the southwest: (a) C^+ along stream-wise direction at $y^+ = 0$ ($= y/L$), (b) C^+ along span-wise direction at $x^+ = 7.5$ ($= x/L$). For wind coming from the west: (c) C^+ along stream-wise direction at $y^+ = 0$ ($= y/L$), (d) C^+ along span-wise direction at $x^+ = 7.5$ ($= x/L$). Symbols: (+): C^+_{ROM} case τ_1; (×): C^+_{ROM} case τ_2; (⊙): C^+_{ROM} case τ_3. Lines: (—): C^+_{CFD} case τ_1; (−−) C^+_{CFD} case τ_2; ($\cdots$) C^+_{CFD} case τ_3.

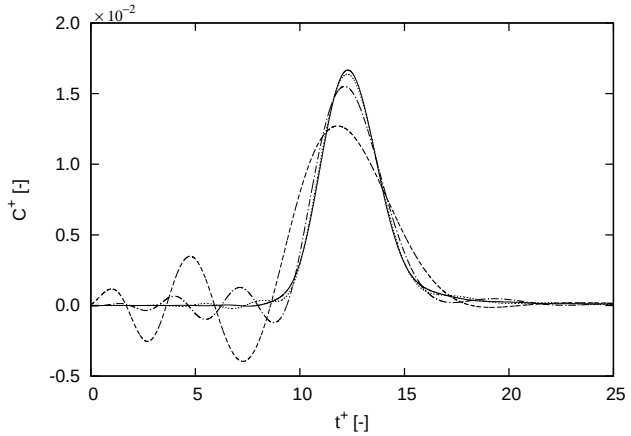

Figure 4: Profiles of the observed dimensionless concentration C^+ (= cUL^2/R) observed at ground level (1 m) at $x^+ = 10$ (= x/L) and $y^+ = 0$ (= y/L) as function of time t^+ (= $(t - t_s)U/L$). Lines: (−−): $r = 25$; (− · −): $r = 50$; (· · ·): $r = 75$; (—): $r = 100$.

while the symbols represent the ROM. The interruptions in the curves between $x^+ = 0 \ldots 1$ and $x^+ = 3.5 \ldots 5.5$ in Fig. 3a, and $x^+ = 0 \ldots 2.5$ in Fig. 3c are due to the presence of buildings and a cooling tower.

Three distinct concentration profiles are found in stream-wise direction for wind coming from the southwest (Fig. 3a). While the stream-wise concentration for case τ_1 shows multiple peaks, the concentration for case τ_3 is rather smooth. Regardless these differences, the ROM is clearly well capable of reproducing these profiles. In span-wise direction (Fig. 3b), a nearly identical span-wise spread of the concentration is found for all three cases but the shape and the magnitude of the profiles are again different. The maximal concentration is found near the centerline although a second peak is found near $x^+ \approx 1$ for case τ_1. Note that around $y^+ = -2.5 \ldots -0.5$, the concentration is also slightly increased due to the part of the plume passing in between the two cooling towers. Again, the profiles predicted by the ROM are indistinguishable from these of the CFD model. The difference between the concentration profiles predicted by the ROM and the CFD model is also negligible for the cases with wind coming from the west. In stream-wise direction (Fig. 3c), the profiles are approximately bell-curved with a maximum at $x^+ \approx 8$ for all three cases. Looking at span-wise direction (Fig. 3d), the concentration profiles are strongly asymmetric but the shape is similar for each of the cases.

In Fig. 4, the effect of changing the order of the ROM on the simulated time evolution of the non-dimensional concentration is shown, observed at ground level at $x^+ = 10$ downwind from the pollutant source ($y^+ = 0$), as a function of the non-dimensional time t^+ for case τ_1 with wind coming from the southwest. Four different orders are considered, i.e. 25, 50, 75 and 100. It is observed that a ROM of order 25 shows large concentration fluctuations prior to the concentration peak at $t^+ = 10 \ldots 15$. In addition, a significantly deviating concentration peak is found. Clearly, a ROM order of 25 is insufficient to reconstruct the concentration profile properly. Increasing the order of the ROM up to 75 steadily decreases both the concentration fluctuations prior to, and the deviation of, the concentration peak.

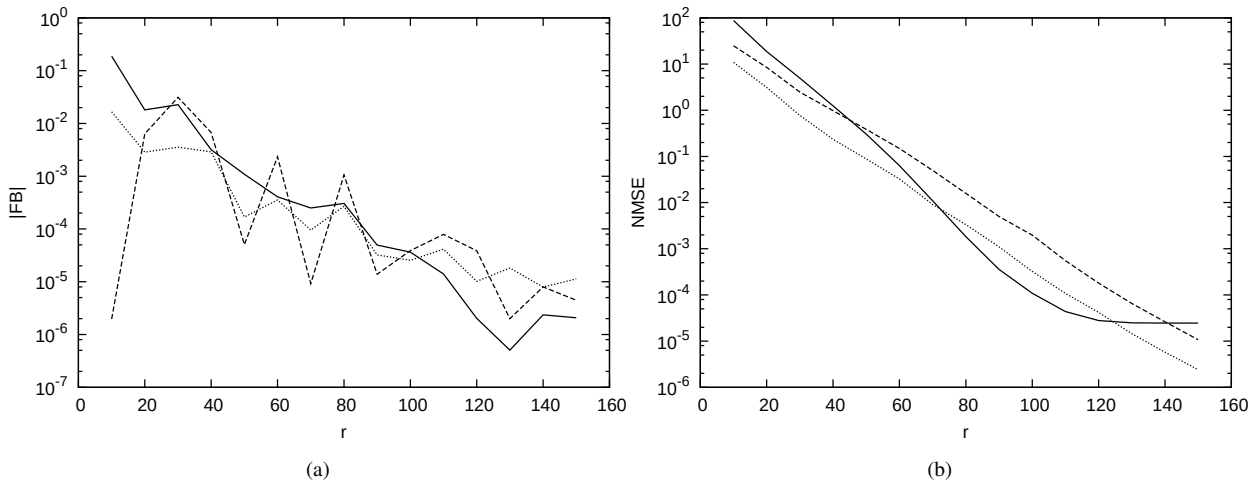

(a) (b)

Figure 5: Performance measures for τ_1 at three time instances. (a) Absolute value of FB, (b) NMSE. Lines: (—): $t^+ = 5$; (−−): $t^+ = 15$; $(\cdots)$: $t^+ = 25$.

At an order of 100, no concentration fluctuations are found and the concentration peak shows very little change with the profile of order 75. For this case, a ROM of order 100 is therefore sufficient for reproducing the concentration profile accurately.

Finally, in Fig. 5, the evolution of the absolute value of FB and the NMSE are shown as function of the order r of the ROM for case τ_1 with wind coming from the southwest at $t^+ = 5$, $t^+ = 15$ and $t^+ = 25$. First of all, it is observed that increasing the order of the ROM improves its accuracy. It is observed that the FB roughly decreases with a reduction rate of one order of magnitude for every addition of 30 to 40 modes. The NMSE decreases more smoothly than FB. For time $t^+ = 5$, the decrease of the NMSE is more than exponential up to $r \approx 120$ after which it stagnates. For $t^+ = 15$ and $t^+ = 25$ a nearly perfect exponential decrease is found at a reduction rate of one order of magnitude for every addition of approximately 20 modes.

4.2. Discussion

CFD is known to be prohibitively expensive with regards to its use for real-time purposes. This is also observed in the current study. Despite the use of 40 CPUs, it still takes 97 s to simulate one second of real time using the CFD model. This is reduced by more than a factor of 2500 to only 38.6 ms per second of real time when the dispersion is simulated using the ROM. In other words, the model runs 25 times faster than real-time. In section §4.1, it is demonstrated that this is without a significant loss in accuracy. Furthermore, when the computational cost is taken into account, i.e. only 1 core is used to for the ROM, the reduction is more than a factor of 10^5.

The construction of the ROM introduces a one-time initialization cost. The bulk of the computational cost is in solving the linear equation $A\tilde{v}_i = v_{i-1}$ using the CFD solver. For each of the r vectors, this is done iteratively using false time-stepping as under-relaxation and requires approximately 720 s. A memory space of $2r \times n$ is required to

store both V and X but this can be freed again after the construction of the ROM. Once set up, the ROM only requires a negligible memory space of r^2, r and $m \times r$ for A_r, B_r and D_r, respectively.

For performing repeated simulations such as in an on-line monitoring context, the advantage of the ROM over the CFD model is clear. However, also for one simulation only the use of the ROM can be interesting. The initialization of one mode of the ROM requires approximately 720 s. The simulation of 1 second of real time requires 97 seconds with the CFD model. Therefore, the time required for the initialization of a ROM with 100 modes equals the simulation of approximately 740 seconds of real time with CFD. Thus, once longer run times are required, it may become interesting to first construct the ROM, and then use it instead for the simulation.

5. Conclusion

In the current study, a reduced order modeling method is introduced which allows to simulate the dispersion of a pollutant in a built environment faster than real-time. To this end, a Krylov-subspace projection-based model reduction method using the Arnoldi algorithm is applied for a CFD model. The method results in a stable ROM, and the algorithm is formulated in such a way that it can be used with any choice of CFD solver. We simulate the pollutant dispersion using an Eulerian approach where the concentration is formulated as a transient three-dimensional advection-diffusion problem on a steady velocity background.

To assess the approach, three cases of a time-dependent pollutant emission are simulated using both the CFD and the ROM. The Doel Nuclear Power Station was selected as the subject of the study. The simulations show that for all of the cases, the ROM is well capable of reconstructing both the shape and the magnitude of the pollutant concentration without significant loss in accuracy. In addition, it is illustrated that increasing the order of the ROM, further increases the accuracy, i.e. the ROM converges towards the CFD model. After initialization, the application of this method resulted in the reduction of the computational time by a factor of 2500, running 25 times faster than real-time. Furthermore, when the computational cost is looked at, the reduction was more than a factor of 10^5.

In the current work, a ROM is constructed for the dispersion of a non-buoyant, non-reactive gas in a steady, thermally neutral boundary layer for one wind direction only. For the extension towards multiple wind directions, it might be interesting to consider parametric model order reduction (see, e.g., Ref. [47]). In case of the occurrence of buoyancy effects due to a temperature difference between the ambient air and the gas emitted, plume rise models could be applied to estimate an effective emission height (see, e.g., Ref. [48]). A non-zero emission velocity can be accounted for in a similar way. Extending the ROM to the dispersion of gases with significantly higher density than air remains a challenge due to the strong, non-linear coupling with the momentum equation. Also the automated selection of a suitable order of the ROM remains challenging (see, e.g., Ref. [33] and Ref. [49]) These are interesting topics for further research.

Acknowledgments

All simulations were carried out using the computing infrastructure of the Flemish Supercomputer Center (VSC), funded by the Hercules Foundation and the Flemish Government. We thank Karl Meerbergen for the useful discussions on model order reduction.

Appendix A. Proof

As stated in §2.2, the same basis V and reduced matrix A_r are produced by Algorithm 1 and Algorithm 2. The equivalence the of basis V is readily seen, since the introduction of X in Algorithm 2 does not affect the construction of V. Thus, Algorithm 2 reduces to Algorithm 1 for the construction of V. The proof that, for any order r, $X^{(r)} = AV^{(r)}$ can be constructed by induction. Here, we use superscript (r) to denote the order of the constructed model. In Algorithm 2 (p5), these superscripts are omitted for sake of brevity.

Base case: when $r = 1$, $V^1 = A^{-1}b/\|\tilde{v}_1\|$ and $X^1 = b/\|\tilde{v}_1\|$ by construction. Hence, $AV^1 = X^1$.

Induction hypothesis: Assume that $AV^{(r-1)} = X^{(r-1)}$ holds for some positive integer r.

Inductive step: We now show that using Algorithm 2, $AV^{(r)} = X^{(r)}$. We have

$$AV^{(r)} = \begin{bmatrix} AV^{(r-1)} & Av_r \end{bmatrix} \tag{A.1}$$

$$= \begin{bmatrix} X^{(r-1)} & Av_r \end{bmatrix} \quad \text{(by induction hypothesis)} \tag{A.2}$$

We further need to show that $Av_r = x_r$. Therefore, we start from writing the orthogonalization of $\tilde{v}_r$ to v_r in Algorithm 2 as

$$v_r = \alpha\tilde{v}_r - [h_1\ h_2\ \ldots\ h_{r-1}]V^{(r-1)} \tag{A.3}$$

Left-multiplying with matrix A gives

$$Av_r = A\left(\alpha\tilde{v}_r - [h_1\ h_2\ \ldots\ h_{r-1}]V^{(r-1)}\right) \tag{A.4}$$

$$= \alpha A\tilde{v}_r - [h_1\ h_2\ \ldots\ h_{r-1}]AV^{(r-1)} \tag{A.5}$$

$$= \alpha\tilde{x}_r - [h_1\ h_2\ \ldots\ h_{r-1}]X^{(r-1)} \tag{A.6}$$

$$= x_r \quad \text{(by construction)} \tag{A.7}$$

where we use $A\tilde{v}_i = \tilde{x}_i$, as defined in Algorithm 2. Thus $AV^{(r)} = X^{(r)}$ for any order r.

[1] E. Sanchez, J. C. Lerner, A. Porta, P. Jacovkis, Accidental release of chlorine in Chicago: Coupling of an exposure model with a computational fluid dynamics model, Atmospheric Environment 64 (2013) 47–55.

[2] J. Tixier, G. Dusserre, S. Rault-Doumax, J. Ollivier, C. Bourely, OSIRIS: software for the consequence evaluation of transportation of dangerous goods accidents, Environmental modelling & software 17 (7) (2002) 627–637.

[3] C. Landman, J. Päsler-Sauer, W. Raskob, The Decision Support System RODOS, in: The Risks of Nuclear Energy Technology, Springer, 337–348, 2014.

[4] Á. Leelőssy, F. Molnár Jr, F. Izsák, Á. Havasi, I. Lagzi, R. Mészáros, Dispersion modeling of air pollutants in the atmosphere: a review, Central European Journal of Geosciences 6 (3) (2014) 257–278.

[5] S. R. Hanna, O. R. Hansen, M. Ichard, D. Strimaitis, CFD model simulation of dispersion from chlorine railcar releases in industrial and urban areas, Atmospheric Environment 43 (2) (2009) 262–270.

[6] Y. Tominaga, T. Stathopoulos, Numerical simulation of dispersion around an isolated cubic building: model evaluation of RANS and LES, Building and Environment 45 (10) (2010) 2231–2239.

[7] B. Blocken, Y. Tominaga, T. Stathopoulos, CFD simulation of micro-scale pollutant dispersion in the built environment, Building and Environment 64 (2013) 225–230.

[8] Y. Tominaga, T. Stathopoulos, CFD simulation of near-field pollutant dispersion in the urban environment: A review of current modeling techniques, Atmospheric Environment 79 (2013) 716–730.

[9] B. Blocken, T. Stathopoulos, P. Saathoff, X. Wang, Numerical evaluation of pollutant dispersion in the built environment: comparisons between models and experiments, Journal of Wind Engineering and Industrial Aerodynamics 96 (10) (2008) 1817–1831.

[10] M. Lateb, C. Masson, T. Stathopoulos, C. Bédard, Numerical simulation of pollutant dispersion around a building complex, Building and Environment 45 (8) (2010) 1788–1798.

[11] P. Gousseau, B. Blocken, T. Stathopoulos, G. Van Heijst, CFD simulation of near-field pollutant dispersion on a high-resolution grid: a case study by LES and RANS for a building group in downtown Montreal, Atmospheric Environment 45 (2) (2011) 428–438.

[12] J. Hang, Y. Li, M. Sandberg, R. Buccolieri, S. Di Sabatino, The influence of building height variability on pollutant dispersion and pedestrian ventilation in idealized high-rise urban areas, Building and Environment 56 (2012) 346–360.

[13] S. R. Hanna, M. J. Brown, F. E. Camelli, S. T. Chan, W. J. Coirier, S. Kim, O. R. Hansen, A. H. Huber, R. M. Reynolds, Detailed simulations of atmospheric flow and dispersion in downtown Manhattan: An application of five computational fluid dynamics models, Bulletin of the American Meteorological Society 87 (12) (2006) 1713–1726.

[14] E. Sanchez, J. C. Lerner, A. Porta, P. Jacovkis, Emergencies planning and response: Coupling an exposure model with different atmospheric dispersion models, Atmospheric Environment 79 (2013) 486–494.

[15] I. Senocak, J. C. Thibault, M. Caylor, Rapid-response urban CFD simulations using a GPU computing paradigm on desktop supercomputers, in: Eighth Symposium on the Urban Environment, J19.2, 2009.

[16] A. A. Gowardhan, E. R. Pardyjak, I. Senocak, M. J. Brown, A CFD-based wind solver for an urban fast response transport and dispersion model, Environmental fluid mechanics 11 (5) (2011) 439–464.

[17] U. Baur, P. Benner, L. Feng, Model order reduction for linear and nonlinear systems: a system-theoretic perspective, Archives of Computational Methods in Engineering 21 (4) (2014) 331–358.

[18] D. J. Lucia, P. S. Beran, W. A. Silva, Reduced-order modeling: new approaches for computational physics, Progress in Aerospace Sciences 40 (1) (2004) 51–117.

[19] A. C. Antoulas, D. C. Sorensen, S. Gugercin, A survey of model reduction methods for large-scale systems, Contemporary mathematics 280 (2001) 193–220.

[20] R. C. Selga, B. Lohmann, R. Eid, Stability preservation in projection-based model order reduction of large scale systems, European Journal of Control 18 (2) (2012) 122–132.

[21] C.-C. Chu, M.-H. Lai, W.-S. Feng, Model-order reductions for MIMO systems using global Krylov subspace methods, Mathematics and computers in Simulation 79 (4) (2008) 1153–1164.

[22] R. W. Freund, Model reduction methods based on Krylov subspaces, Acta Numerica 12 (2003) 267–319.

[23] B. Philippe, L. Reichel, On the generation of Krylov subspace bases, Applied Numerical Mathematics 62 (9) (2012) 1171–1186.

[24] B. Nour-Omid, W. Dunbar, A. Woodbury, Lanczos and Arnoldi methods for the solution of convection-diffusion equations, Computer methods in applied mechanics and engineering 88 (1) (1991) 75–95.

[25] A. D. Woodbury, W. S. Dunbar, B. Nour-Omid, Application of the Arnoldi Algorithm to the solution of the advection-dispersion equation, Water resources research 26 (10) (1990) 2579–2590.

[26] K. Zhang, A. D. Woodbury, A Krylov finite element approach for multi-species contaminant transport in discretely fractured porous media, Advances in water resources 25 (7) (2002) 705–721.

[27] K. Willcox, J. Peraire, J. White, An Arnoldi approach for generation of reduced-order models for turbomachinery, Computers & fluids 31 (3) (2002) 369–389.

[28] Y. Wang, H. Song, K. Pant, A reduced-order model for whole-chip thermal analysis of microfluidic lab-on-a-chip systems, Microfluidics and nanofluidics 16 (1-2) (2014) 369–380.

[29] Y. Tominaga, T. Stathopoulos, Turbulent Schmidt numbers for CFD analysis with various types of flowfield, Atmospheric Environment 41 (37) (2007) 8091–8099.

[30] R. S. Puri, D. Morrey, A Krylov–Arnoldi reduced order modelling framework for efficient, fully coupled, structural–acoustic optimization, Structural and Multidisciplinary Optimization 43 (4) (2011) 495–517.

[31] B. Salimbahrami, B. Lohmann, Krylov subspace methods for the reduction of first and second order large-scale systems, in: Proc. of 8th DFMRS conference, 236–251, 2004.

[32] J. Liesen, Z. Strakos, Krylov subspace methods: principles and analysis, Oxford University Press, 2012.

[33] B. Salimbahrami, B. Lohmann, T. Bechtold, J. Korvink, Two-sided Arnoldi algorithm and its application in order reduction of MEMS, in: Proc. 4th Mathmod, Citeseer, 1021–1028, 2003.

[34] R. S. Puri, D. Morrey, J. L. Cipolla, A comparison between one-sided and two-sided Arnoldi-based model order reduction (MORe) techniques for fully coupled structural-acoustic analysis, The Journal of the Acoustical Society of America 121 (5) (2007) 3097–3097.

[35] L. M. Silveira, M. Kamon, I. Elfadel, J. White, A coordinate-transformed Arnoldi algorithm for generating guaranteed stable reduced-order models of {RLC} circuits, Computer Methods in Applied Mechanics and Engineering 169 (3–4) (1999) 377–389.

[36] I. M. Jaimoukha, E. M. Kasenally, Implicitly restarted Krylov subspace methods for stable partial realizations, SIAM Journal on Matrix Analysis and Applications 18 (3) (1997) 633–652.

[37] D. Amsallem, C. Farhat, Stabilization of projection-based reduced-order models, International Journal for Numerical Methods in Engineering 91 (4) (2012) 358–377.

[38] J. Chang, S. Hanna, Air quality model performance evaluation, Meteorology and Atmospheric Physics 87 (1-3) (2004) 167–196.

[39] L. Vervecken, J. Camps, J. Meyers, Accounting for wind-direction fluctuations in Reynolds-averaged simulation of near-range atmospheric dispersion, Atmospheric Environment 72 (2013) 142–150, doi:10.1016/j.atmosenv.2013.03.005.

[40] B. E. Launder, D. Spalding, The numerical computation of turbulent flows, Computer methods in applied mechanics and engineering 3 (2) (1974) 269–289.

[41] P. Richards, R. Hoxey, Appropriate boundary conditions for computational wind engineering models using the k-ϵ turbulence model, Journal of wind engineering and industrial aerodynamics 46 (1993) 145–153.

[42] S. Balay, W. D. Gropp, L. C. McInnes, B. F. Smith, Efficient Management of Parallelism in Object Oriented Numerical Software Libraries, in: E. Arge, A. M. Bruaset, H. P. Langtangen (Eds.), Modern Software Tools in Scientific Computing, Birkhäuser Press, 163–202, 1997.

[43] S. Balay, S. Abhyankar, M. F. Adams, J. Brown, P. Brune, K. Buschelman, V. Eijkhout, W. D. Gropp, D. Kaushik, M. G. Knepley, L. C. McInnes, K. Rupp, B. F. Smith, H. Zhang, PETSc Users Manual, Tech. Rep. ANL-95/11 - Revision 3.5, Argonne National Laboratory, URL `http://www.mcs.anl.gov/petsc`, 2014.

[44] S. Balay, S. Abhyankar, M. F. Adams, J. Brown, P. Brune, K. Buschelman, V. Eijkhout, W. D. Gropp, D. Kaushik, M. G. Knepley, L. C. McInnes, K. Rupp, B. F. Smith, H. Zhang, PETSc Web page, `http://www.mcs.anl.gov/petsc`, URL `http://www.mcs.anl.gov/petsc`, 2014.

[45] M. Chavez, B. Hajra, T. Stathopoulos, A. Bahloul, Near-field pollutant dispersion in the built environment by CFD and wind tunnel simulations, Journal of Wind Engineering and Industrial Aerodynamics 99 (4) (2011) 330–339.

[46] L. Vervecken, J. Camps, J. Meyers, Dynamic dose assessment by Large Eddy Simulation of the near-range atmospheric dispersion, Journal of Radiological Protection 35 (1) (2015) 165–178, doi:10.1088/0952-4746/35/1/165.

[47] H. Panzer, J. Mohring, R. Eid, B. Lohmann, Parametric model order reduction by matrix interpolation, at-Automatisierungstechnik Methoden und Anwendungen der Steuerungs-, Regelungs-und Informationstechnik 58 (8) (2010) 475–484.

[48] N. Kozarev, N. Ilieva, E. Sokolovski, Full scale plume rise modeling in calm and low wind velocity conditions, Clean Technologies and

Environmental Policy 16 (3) (2014) 637–645.

[49] M. Bazaz, S. Janardhanan, et al., A stopping criterion for Krylov-subspace based model order reduction techniques, in: Modelling, Identification & Control (ICMIC), 2012 Proceedings of International Conference on, IEEE, 921–925, 2012.